CrystEngComm

Cite this: *CrystEngComm*, 2011, **13**, 2955

www.rsc.org/crystengcomm

PAPER

Crystalline Te nanotube and Te nanorods-on-CdTe nanotube arrays on ITO *via* a ZnO nanorod templating-reaction

Xina Wang,[ab] Yeming Xu,[b] Haojun Zhu,[b] Rong Liu,[a] Hao Wang*[a] and Quan Li[b]

Received 5th January 2011, Accepted 8th February 2011
DOI: 10.1039/c1ce00010a

Vertically aligned Te nanotube and CdTe nanotube arrays branched with Te nanorods were demonstrated on an indium tin oxide (ITO) substrate *via* a ZnO nanorods templating-reaction method. By simply changing the etchant type and etching temperature of the ZnO–CdTe core–shell nanocables, the ZnO cores can be selectively etched off and the chemical reaction from CdTe to Te can be well controlled to form pure CdTe or Te nanotubes, or Te nanorods-on-CdTe nanotube nanocomposite arrays. Both the well-crystallized Te nanotubes and the Te nanorods are of hexagonal phase, of which the former have respective wall thickness, diameter and length of ~60 nm, ~150 nm and ~8 μm, and the latter have diameter and length of ~17 nm and ~80 nm. Dynamic studies on the structural and morphological evolution from ZnO–CdTe nanocables to the Te-related nanostructures were performed. The formation mechanism of the Te nanorods-on-CdTe nanotube arrays and pure Te and/or CdTe nanotube arrays are discussed.

Introduction

Recently, one-dimensional (1D) semiconductor nanostructures including nanotubes, nanowires, and nanobelts have attracted great research interest because of their superior electronic, optical, catalytic and mechanical properties compared to their thin film and/or bulk counterparts.[1] Among the various 1D nanostructures, semiconductor nanotubes, which combine tubular morphology with the unique physical properties of semiconductors, have great potential to serve as functional building blocks for nanodevices.[2] In particular, when nanotubes were integrated with a second material to construct heterostructure nanocomposites, better and broader applications can be expected due to the tunable chemical reactivity and physical properties.[3] For example, core–sheath heterostructure TiO_2–CdS and TiO_2–$SrTiO_3$ nanotube arrays have been constructed for application in photoelectrochemical cells,[4] while enhanced photocatalytic properties have been found by fabricating TiO_2–Pt coaxial nanotube arrays and graphitized carbon nanotubes-in-TiO_2 nanotube arrays.[5] However, compared with the numerous studies on coaxial nanocables based on nanowires and nanorods, such as ZnO–CdSe, ZnO–CdTe, GaP–SiO_x, ZnS–SiO_x, ZnS–Zn, Si–TiO_2, and Pb–ZnO core–shell nanocables,[6] nanotube heterocomposites have been restricted to the TiO_2 system, which has greatly limited application due to its large band gap. On the other hand, the formation of TiO_2 nanotube-based heterostructures usually contains a two-step process, in which the TiO_2 nanotube arrays are prefabricated by electrochemical anodization of Ti foil or AAO-templating electrodeposition, and the latter material is formed on the former through electrodeposition, annealing or hydrothermal processing in the atmosphere composed of the precursor.[4,5] As the formation of ordered TiO_2 nanotube arrays relies heavily on the anodization or electrodeposition conditions, while the two-step route increases the complexity of the fabrication process, other methods should be explored for the formation of semiconductor nanotubes and nanocomposites.

As an elemental semiconductor with band gap of 0.35 eV, tellurium (Te) has broad applications in electronic and optoelectronic devices due to its promising properties including nonlinear optical response, photoconductivity, thermoelectricity and piezoelectric effects.[7] Various Te nanostructures including nanoneedles, nanowires, nanorods, nanotubes and nanobelts have been extensively fabricated through the solution route and the electrodeposition method.[8] Nevertheless, many real device applications require the ordering of nanostructure assemblies into arrays on a conducting substrate. In this regard, the fabrication of aligned Te nanotube arrays on conducting substrates remains challenging. On the other hand, as Te-based 1D core–shell heterostructures such as Te–carbon, Te–Bi, and Te–Bi_2Te_3 nanocables have been fabricated,[9] its integration with other functional nanotubes (such as narrow-gap semiconductor nanotubes) should also be explored.

In the present work, a ZnO nanorod templating-reaction method was proposed for the fabrication of Te nanotube arrays and 1D nanocomposite arrays of Te with CdTe, an important semiconductor which has wide applications in photovoltaics, sensors and detectors because of its band-gap of 1.5 eV and high

[a]*Faculty of Physics and Electronic Technology, Hubei University, Wuhan, 430062, China. E-mail: nanoguy@126.com; Tel: +86 27 8866 2550*
[b]*Department of Physics, The Chinese University of Hong Kong, ShatinNew Territory, Hong Kong, China*

optical absorption, atomic number and electron density.[10] By simply soaking ZnO–CdTe nanocable arrays-on-ITO samples in ammonia solution, Te nanorods-on-CdTe nanotube arrays can be formed through the synchronous etching of the ZnO nanorod cores with partial reduction of the CdTe shells to Te. Pure Te nanotube arrays can be achieved on ITO substrates by adjusting the etching conditions of the ZnO–CdTe nanocable arrays. Detailed characterization of the sample morphology, structure and composition were performed, together with the morphology evolution during the etching and reaction process based on the formation mechanism for both the pure Te and the hetero-structure nanotube arrays.

Experimental

Pure Te nanotube arrays and Te nanorods-on-CdTe nanotube arrays were synthesized *via* a ZnO nanorod templating-reaction method under different etching conditions. ZnO–CdTe nanocable arrays-on-ITO precursors were prefabricated by electrodepositing CdTe nanoshells onto ZnO nanorod arrays on ITO with a standard three-electrode system at room temperature, for which details can be found in ref. 6*b*. The electrolyte was a neutral pH (8.0–8.5) aqueous solution containing 0.05 M nitrilotriacetic acid trisodium salt (NTA), 0.005 M potassium tellurite (K_2TeO_3), and 0.02 M cadmium acetate. The pH value and NTA concentration of the remnant electrolyte changed little after the electrodeposition. The ZnO–CdTe nanocable arrays samples were dipped into the remnant NTA electrolyte at 70 °C for 0.5 h and 1 h, respectively. As a comparison, another ZnO–CdTe nanocable array sample was sunk into a 25% ammonia aqueous solution at 50 °C for 1 h. After etching, the samples were cleaned with de-ionized water and dried with a flow of nitrogen. The crystal structure and composition of the samples were studied by X-ray powder diffraction (XRD, Rigaku model RU300) using the Cu Kα1 line. The morphology and structure of the samples were characterized using field-emission scanning electron microscopy (FE–SEM, FEI Quantum F400) and (scanning) transmission electron microscopy (STEM, TEM, Tecnai Model 20 FEG) equipped with an energy dispersive X-ray (EDX) spectrometer, respectively. High-resolution TEM (HRTEM), selective area electron diffraction (SAED), and EDX characterization were performed to study the microstructure and elemental composition of the samples.

Results and discussion

Synthesis of nanotube arrays

The formation of Te nanotube arrays can be illustrated as the following steps. Firstly, using ZnO nanorod arrays on ITO as initial template (Fig. 1a), CdTe nanocrystal shells were electrodeposited onto the surface of ZnO nanorods to form a core–shell ZnO–CdTe nanocable structure (Fig. 1b). In this series, the diameter of the ZnO nanorods is 150 ± 14 nm, and the thickness of the CdTe nanocrystal shells is ~70 nm. As the shell thickness is less than the radius of the ZnO nanorod, the top surfaces of the nanocables were partially covered with CdTe. Compared with the hexagonal structure of ZnO nanorods which show $\{10\bar{1}0\}$ planes as side surfaces and {0002} planes as top surfaces, the surfaces of the nanocables are much rougher, although the shells

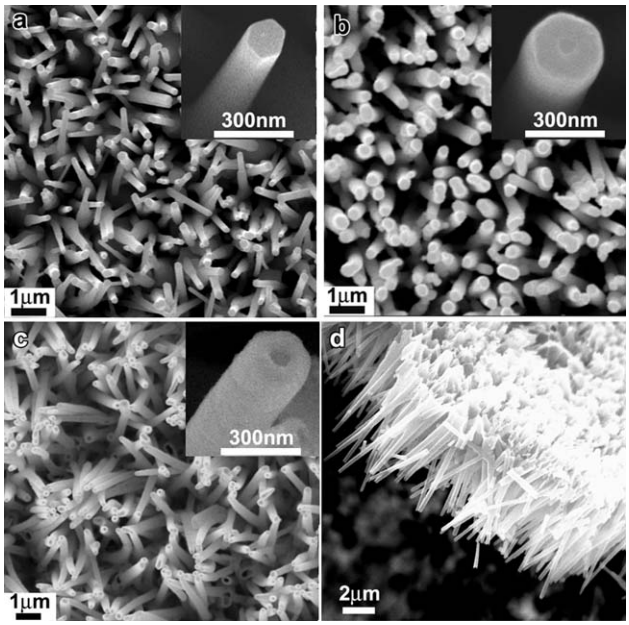

Fig. 1 SEM images of (a) pure ZnO nanorod arrays, (b) ZnO–CdTe nanocable arrays, (c) and (d) Te nanotube arrays on ITO after etching of the ZnO–CdTe nanocables by remnant NTA electrolyte, the insets show the corresponding magnified SEM images.

are very homogeneous along the axial direction. Then, the etching process of the ZnO–CdTe nanocables in the remnant NTA electrolyte at 70 °C directly leads to the formation of Te nanotube arrays (Fig. 1c). Though Cd^{2+} cations were also removed from the nanoshells with the etching of ZnO nanorods, the remnant Te species remain in an aligned nanotube array configuration. The inner diameter of the Te nanotubes is ~150nm, consistent with that of the original ZnO nanorods. Compared with the original thickness of CdTe shells, the wall thickness of the Te nanotubes is decreased to ~60 nm, indicating a ~10 nm loss of thickness on going from CdTe nanoshells to Te nanotubes. From the side view of the Te nanotube arrays (Fig. 1d), the length of Te nanotubes is ~8 μm, which depends on that of the initial ZnO template.

The detailed structure and chemical composition of the Te nanotube arrays were further studied by TEM-related techniques (Fig. 2). After the NTA etching of ZnO–CdTe nanocables, a distinct tubular structure with open ends can be clearly seen in Fig. 2a. As shown by the corresponding EDX spectrum (Fig. 2b), the nanotube is mainly composed of Te, while the signals of Cd and Zn can be neglected. The SAED pattern (inset Fig. 2a) taken from the as-prepared Te nanotube reveals its polycrystalline nature, although the Te nanocrystals have good crystalline quality as suggested from the bright diffraction dots. The diffraction rings can be indexed to the (100), (101), (102) and (110) planes of the hexagonal structure of Te (JCPDS Card No. 36-1452). After annealing at 200 °C in Ar atmosphere, the diffraction dots become much brighter and more remarkable while the diffraction rings weaker (not shown here), indicating the improvement of the crystal quality and nanocrystal size. This is consistent with the HRTEM images of the as-prepared (Fig. 2c) and post-annealed (Fig. 2d) Te nanotube arrays,

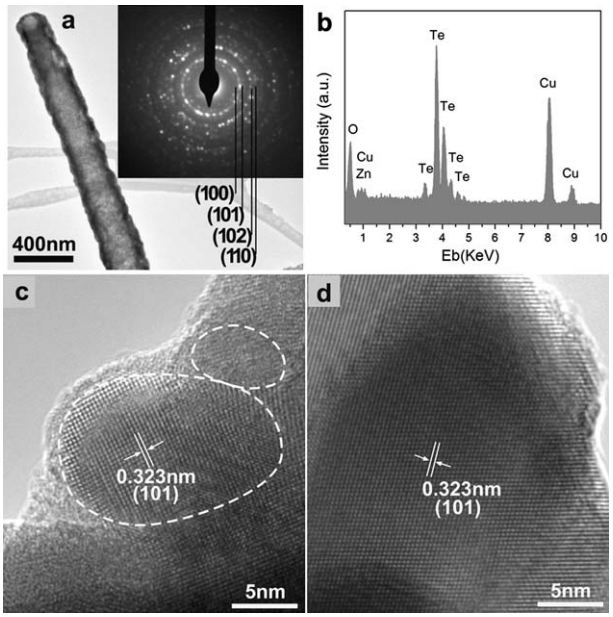

Fig. 2 (a) Low-magnification TEM image of a single Te nanotube; the inset shows the corresponding SAED pattern, (b) EDX spectrum of the Te nanotube, (c) and (d) high-resolution TEM images taken from an as-prepared and a post-annealed Te nanotube, respectively.

respectively. For the as-synthesized sample, the nanocrystals size is less than 10 nm, while it can increase to >20 nm after annealing. The lattice spacing in the HRTEM image is measured as 0.323 nm, corresponding well with the (101) plane of the hexagonal Te.

The structure of the post-annealed Te nanotube arrays were also studied by XRD (Fig. 3). Besides the diffraction peaks of the ITO substrate underneath and the ZnO seed layer grown before the ZnO nanorods, the reflection peaks can be indexed to the hexagonal structure of Te (JCPDS Card No. 36-1452) with cell constants $a = 0.4458$ nm and $c = 0.5927$ nm, which agrees well with the above TEM results. No other peaks have been detected, indicating the annealing process in Ar can effectively avoid the oxidation of Te.

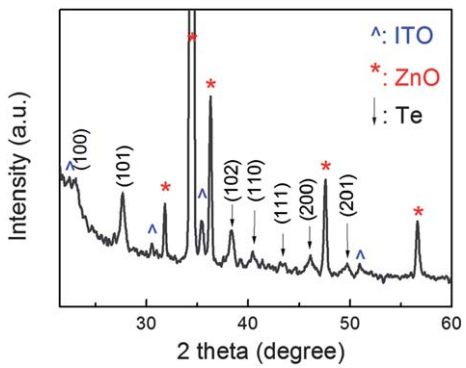

Fig. 3 XRD pattern of the post-annealed Te nanotube arrays on ITO substrate, in which the ZnO signal comes from the ZnO seed layers underneath the Te nanotubes.

Effect of etchant

The etchant type is found to be crucial for the morphology of the final Te related nanostructures. When hot ammonia solution was used to etch the ZnO–CdTe nanocable arrays, CdTe nanotube arrays branched with Te nanorods will form on the ITO substrate. For a ZnO–CdTe nanocable array sample (Fig. 4b) with a core diameter of ~160 nm (Fig. 4a) and a shell thickness of ~90 nm, after being soaked in ammonia at 50 °C for 1 h, the nanorod cores were totally etched off, leaving the shells in a nanotube configuration. At the same time, the growth of many nanorods ~17 nm in diameter and ~80 nm in length can be clearly found on the nanotubes' side walls (Fig. 4c and 4d). As revealed by the bright, dark field TEM image (Fig. 5a and 5b) and corresponding EDX spectra (Fig. 5c and 5d), the nanotubes are mainly composed of Cd and Te (Cd : Te ratio ≈ 1) and the branched nanorod of Te. Fig. 5e is the high-magnification TEM image of the nanorods, in which the *d*-spacing of the lattice fringes are measured as 0.223 and 0.235 nm, matching those of the (110) and (102) planes of hexagonal Te (JCPDS Card No. 36-1452), respectively. On the other hand, the HRTEM study demonstrates that the CdTe nanotubes are of a polycrystalline nature. As one can see in Fig. 5f, the lattice spacing of 0.37 nm matches well with the *d*-spacing of the (111) planes of zinc-blende CdTe (JCPDS Card No. 65-880).

For the CdTe shells that were directly exposed to the 70 °C solution of NTA, Cd^{2+} cations can be removed very easily *via* the chelation reaction of NTA^{3-} with CdTe: $CdTe + NTA^{3-} = CdNTA^{-} + Te^{2-}$. Due to the high reducibility of Te^{2-}, it can be oxidized to form Te in the presence of oxygen from the air: $2Te^{2-} + O_2 + 2H_2O = 2Te + 4OH^{-}$.[8a] However, as the ZnO cores are unexposed or partially exposed to the etchant, their detailed etching process is not clear. Subsequently, a dynamic study on the morphology evolution was performed for two typical structures by recording SEM images at different stages of the etching

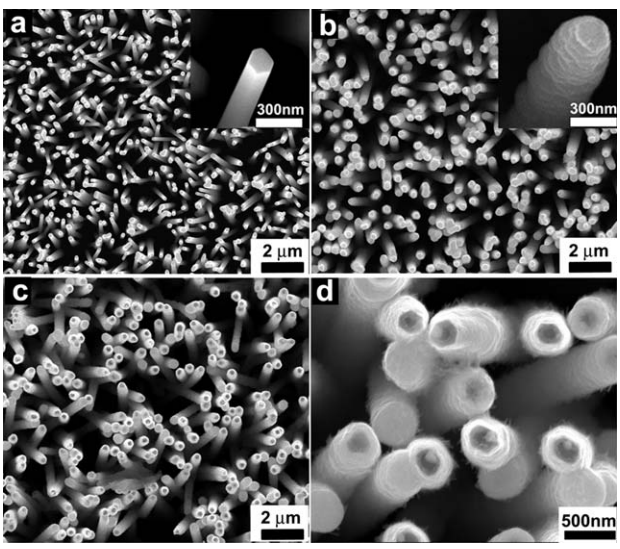

Fig. 4 (a) ZnO nanorod arrays, (b) ZnO–CdTe nanocable arrays, and (c) and (d) low and high magnification SEM images of CdTe nanotube arrays branched with Te nanorods after the nanocables were etched by hot ammonia.

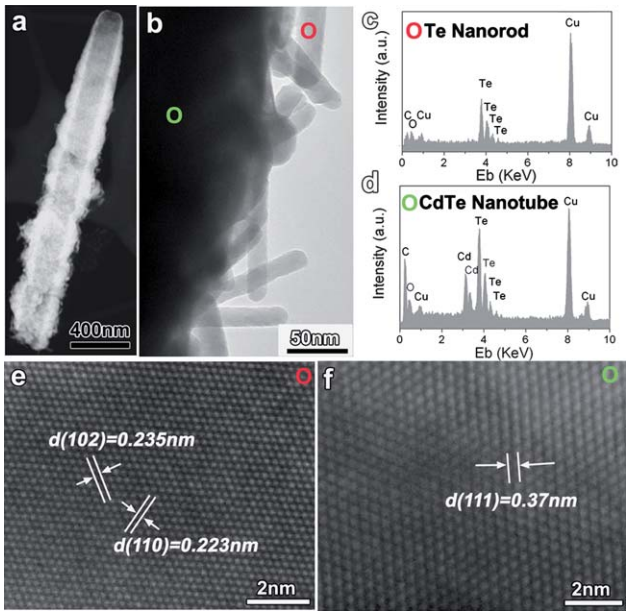

Fig. 5 (a) Bright and (b) dark field TEM images of a single CdTe nanotube branched with Te nanorods, (c) and (d) the EDX spectra taken from different circled regions as shown in (b); (e) and (f) show the corresponding high-resolution TEM images of the Te nanorod and CdTe nanotube, respectively.

process (Fig. 6). For ZnO–CdTe nanocable arrays with partially covered ZnO tops (Fig. 6a), obvious removal of ZnO started along the ZnO–CdTe interfaces after soaking for 0.5 h in remnant NTA electrolyte (Fig. 6b), resulting in a continually expanded empty spacing for the etchant solution to follow in. After 1 h, both the ZnO cores and Cd species were totally etched off and formed Te nanotubes (Fig. 6c). For ZnO–CdTe nanocables with fully covered tops (Fig. 6d), though the top surface of ZnO was not exposed to the etchant, Te cuvettes, *i.e.*, nanotubes

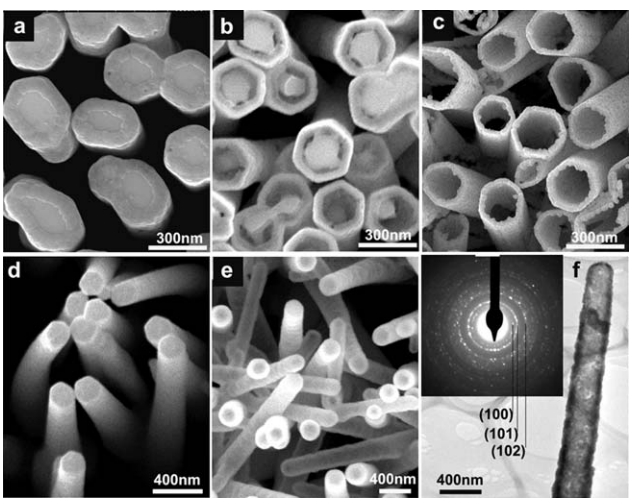

Fig. 6 Time-dependent morphology evolution from ZnO–CdTe nanocables to Te nanotube arrays at different etching times by NTA: (a) 0 h, (b) 0.5 h, and (c) 1 h, (d) and (e) SEM images of ZnO–CdTe nanocables with closed endings and Te nanocuvette arrays formed after etching for 1 h, (f) TEM image of a single Te nanocuvette, and the inset shows the corresponding SAED pattern.

with closed endings, still formed after etching for 1 h (Fig. 6e). As suggested by the corresponding TEM image, the entire Te cuvette has a very continuous wall. Therefore, NTA^{3-} anions can permeate through the CdTe shells to the ZnO cores, then remove the cores through chelation with ZnO which forms a water-soluble zinc nitriloacetate complex: $ZnO + NTA^{3-} + H_2O = ZnNTA^{-} + 2OH^{-}$.

Discussion of the mechanism

In fact, as revealed by our earlier study (ref. 6*b*), the CdTe nanoshells of the as-prepared ZnO–CdTe nanocables are composed of many small nanocrystals with a lot of crystal boundaries and defects, which can provide easy permeation channels for the etchant to react with ZnO from the interface to the cores. This is very similar to the selective etching of Zn–ZnO core–shell nanoparticles, in which the grain boundaries in the shell layer can provide effective diffusion channels for the etchant to enter the core part and preferentially etch the cores.[11] Accordingly, scheme A (Fig. 7) was proposed to illustrate the formation mechanism of Te nanotubes, in which the chelation reactions of NTA^{3-} with ZnO and CdTe can effectively dissolve the ZnO cores as well as remove the Cd species from the nanocables. Furthermore, as the reactions proceed in a relatively mild way, the Te species still maintain the nanotube morphology. Since the CdTe nanoshells before etching process are of a zinc-blende structure with JCPDS Card No. 65-880 (ref. 6*b*), the Te atoms should re-crystalize to form many nanocrystals of hexagonal structure after the Cd atoms are removed, and the ionic Cd–Te bonds should be replaced by Te–Te bonds accordingly.

A different formation mechanism, scheme B (in Fig. 7), which consists of two processes related to the reaction of ZnO–CdTe with ammonia, was also shown for the formation of Te nanorods-on-CdTe nanotubes. On one hand, in a similar manner to the etching process in NTA, the ammonia solution can permeate through CdTe shells and "dissolve" ZnO through reaction with the ammonia *via* the formation of a zinc tetraamine complex: $ZnO + 4NH_3 \cdot H_2O = Zn(NH_3)_4^{2+} + 2OH^{-} + 3H_2O$.[12] On the other hand, ammonia can react with the CdTe shells to form

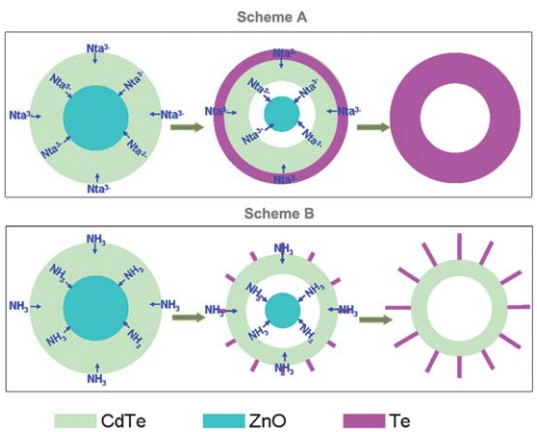

Fig. 7 Schematic illustration of the formation mechanism of Te nanotubes (Scheme A) and Te nanorods-on-CdTe nanotubes (Scheme B) from ZnO–CdTe nanocables under different etching conditions.

a cadmium tetraamine complex: $CdTe + 6NH_3 = Cd(NH_3)_6^{2+} + Te^{2-}$, then the Te^{2-} anions can be oxidized by oxygen to form Te: $Te^{2-} + O^2 + 2H_2O = Te + 4OH^-$.[8a] Compared with NTA^{3-}, the reaction rate of ammonia with CdTe is much slower. As suggested by Fig. 4 and Fig. 5, the thickness of CdTe was reduced to ~75 nm from the initial ~90 nm after 1 h reaction with ammonia, *i.e.*, only ~15 nm-thick CdTe being depleted for the Te nanorods. As long as these reactions proceed slowly enough, Te nanocrystals can grow larger and longer to form single-crystal Te nanorods.[8a] Furthermore, because the reaction of ammonia with ZnO is mild enough, the unreacted CdTe can remain in the nanotube arrays morphology, and thus serve as a good template for the nucleation and growth of the Te nanorods. When the ZnO cores were totally "dissolved", CdTe nanotubes branched with many Te nanorods would form on a ITO substrate.

Effect of temperature

The temperature of the etching solution is found to be another crucial factor affecting the morphology of the final products. When ZnO–CdTe nanocable arrays were soaked in an aqueous ammonia solution at room temperature for 1 h, pure CdTe nanotube arrays will form on ITO, the absence of any Te nanorods indicating that the reactivity of CdTe with ammonia is very low. When soaked in the NTA etchant below 50 °C, little change can be observed for ZnO–CdTe nanocable arrays even after 2 h soaking, suggesting that the chelation reactions of NTA with ZnO and CdTe occur very slowly. Therefore, by controlling the etchant type and temperature, Te nanotube and CdTe nanotube arrays with or without Te nanorods can be obtained respectively.

Conclusion

A series of Te-related arrays have been achieved on ITO by a ZnO nanorod templating-reaction method under different etching conditions. The mild chelation reaction of NTA^{3-} with ZnO–CdTe nanocables contributes to the formation of hexagonal Te nanotube arrays. The effective dissolution of ZnO in ammonia and temperature-dependent reactivity of CdTe with ammonia determine the growth of Te nanorods on the unreacted CdTe nanotubes, which serves as a good nucleation template. By controlling the structure of the ZnO–CdTe nanocables, such as shell thickness, and the diameter and length of ZnO nanorods, size controllable Te nanotube arrays and Te nanorods-on-CdTe nanotube arrays can be expected, which may be required for various nanodevice applications, such as gas sensors, field-effect devices, infrared acoustooptic deflectors and solar cells.

Acknowledgements

This work is supported in part by the National Nature Science Foundation of China (No.51072049), Research Fund for the Doctoral Program of Higher Education of China (RFDP, No. 20104208120004), NSF and ED of Hubei Province (Nos.2009CDA035, Z20091001 and R20101006).

References

1 (*a*) K. Zhu, N. R. Neale, A. Miedaner and A. J. Frank, *Nano Lett.*, 2007, **7**, 69; (*b*) P. A. Sergiu, G. Andrei, M. Jan, H. Robert and S. Patrik, *Nano Lett.*, 2007, **7**, 1286; (*c*) M. H. Huang, S. Mao, H. Feick, H. Q. Yan, Y. Y. Wu, H. Kind, E. Weber, R. Russo and P. D. Yang, *Science*, 2001, **292**, 1897; (*d*) Y. Cui, Q. Q. Wei, H. K. Park and C. M. Lieber, *Science*, 2001, **293**, 1289; (*e*) Z. W. Pan, Z. R. Dai and Z. L. Wang, *Science*, 2001, **291**, 1947.

2 C. N. R. Rao and A. Govindaraj, *Nanotubes and Nanowires*, RSC Publishing, Cambridge, UK, 2005.

3 (*a*) U. K. Gautam, X. Fang, Y. Bando, J. Zhan and D. Golberg, *ACS Nano*, 2008, **2**, 1015; (*b*) H.-C. Liao, P.-C. Kuo, C.-C. Lin and S.-Y. Chen, *J. Vac. Sci. Technol., B: Microelectron. Nanometer Struct.–Process., Meas., Phenom.*, 2006, **24**, 2198; (*c*) D. Yang, G. Meng, S. Zhang, Y. Hao, X. An, Q. Wei, M. Ye and L. Zhang, *Chem. Commun.*, 2007, (17), 1733; (*d*) T. Djenizian, I. Hanzu and Y. D. Premchand, *Nanotechnology*, 2008, **19**, 205601; (*e*) S. K. Mohapatra, S. Banerjee and M. Misra, *Nanotechnology*, 2008, **19**, 315601.

4 (*a*) Y. Yin, Z. Jin and F. Hou, *Nanotechnology*, 2007, **18**, 495608; (*b*) J. Zhang, J. H. Bang, C. Tang and P. V. Kamat, *ACS Nano*, 2010, **4**, 387.

5 (*a*) L. Yang, S. Luo, S. Liu and Q. Cai, *J. Phys. Chem. C*, 2008, **112**, 8939; (*b*) H. Chen, S. Chen, X. Quan, H. Yu, H. Zhao and Y. Zhang, *J. Phys. Chem. C*, 2008, **112**, 9285.

6 (*a*) C. Lévy-Clément, R. Tema-Zaera, M. A. Ryan, A. Katty and G. Hodes, *Adv. Mater.*, 2005, **17**, 1512; (*b*) X. N. Wang, H. J. Zhu, Y. M. Xu, Y. Tao, S. K. Hark, X. D. Xiao and Q. Li, *ACS Nano*, 2010, **4**, 3302; (*c*) S. Y. Bae, H. W. Seo, H. C. Choi, D. S. Han and J. Park, *J. Phys. Chem. B*, 2005, **109**, 8496; (*d*) X. Fan, M. Meng, X. H. Zhang and S. K. Wu, *Appl. Phys. Lett.*, 2005, **86**, 173111; (*e*) Y. C. Zhu, Y. Bando and Y. Uemura, *Chem. Commun.*, 2003, (7), 836; (*f*) Y. J. Hwang, A. Boukai and P. D. Yang, *Nano Lett.*, 2009, **9**, 410; (*g*) C. Y. Wang, N. W. Gong and L. J. Che, *Adv. Mater.*, 2008, **20**, A1.

7 (*a*) R. Beauvais, A. Lessard, P. Galarneau and E. J. Knystautas, *Appl. Phys. Lett.*, 1990, **57**, 1354; (*b*) V. B. Anain, Y. V. Kosichk, A. T. Nadezhdinskii and A. M. Shirokov, *Phys. Status Solidi A*, 1973, **20**, 253; (*c*) D. Royer and E. Dieulesaint, *J. Appl. Phys.*, 1979, **50**, 4042; (*d*) V. Damodaradas, N. Jayaprakash and N. Soundararajan, *J. Mater. Sci.*, 1981, **16**, 3331; (*e*) Z. Wlodek, *Phys. Rev. Lett.*, 1974, **32**, 1373.

8 (*a*) Z. Deng, D. Chen, F. Q. Tang and M. Mansuripur, *Cryst. Growth Des.*, 2009, **9**, 1823; (*b*) Z. Y. Tang, Y. Wang, K. Sun and N. A. Kotov, *Adv. Mater.*, 2005, **17**, 358; (*c*) G. Xi, Y. Peng, W. Yu and Q. Tian, *Cryst. Growth Des.*, 2005, **5**, 325; (*d*) H.-Y. Tuan and B. A. Korgel, *Cryst. Growth Des.*, 2008, **8**, 2555; (*e*) Z. Liu, Z. Hu, J. Liang, S. Li, Y. Yang, S. Peng and Y. Qian, *Langmuir*, 2004, **20**, 214; (*f*) G. She, W. Shi, X. Zhang, T. Wong, Y. Cai and N. Wang, *Cryst. Growth Des.*, 2009, **9**, 663; (*g*) B. Mayers and Y. Xia, *Adv. Mater.*, 2002, **14**, 279; (*h*) J. M. Song, Y. Z. Lin, Y. J. Zhan, Y. C. Tian, G. Liu and S. H. Yu, *Cryst. Growth Des.*, 2008, **8**, 1902; (*i*) M. Mo, J. Zeng, X. Liu, W. Yu, S. Zhang and Y. Qian, *Adv. Mater.*, 2002, **14**, 1658.

9 (*a*) W. Wang, L. Sun, Z. Fang, L. Chen and Z. Zhang, *Cryst. Growth Des.*, 2009, **9**, 2117; (*b*) G. Zhang, W. Wang and X. Li, *Adv. Mater.*, 2008, **20**, 3654.

10 (*a*) I. Visoly-Fisher, S. R. Cohen, A. Ruzin and D. Cahen, *Adv. Mater.*, 2004, **16**, 879; (*b*) N. N. Mamedova, N. A. Kotov, A. L. Rogach and J. Studer, *Nano Lett.*, 2001, **1**, 281.

11 (*a*) H. B. Zeng, W. P. Cai, P. S. Liu, X. X. Xu, H. J. Zhou, C. Klingshirn and H. Kalt, *ACS Nano*, 2008, **2**, 1661; (*b*) H. B. Zeng, P. S. Liu, W. P. Cai, S. K. Yang and X. X. Xu, *J. Phys. Chem. C*, 2008, **112**, 19620.

12 M. J. Zhou, H. J. Zhu, X. N. Wang, Y. M. Xu, Y. Tao, S. K. Hark, X. D. Xiao and Q. Li, *Chem. Mater.*, 2010, **22**, 64.